Preventive Public Safety Power Shutoff Planning under Decision-Dependent Wildfire Ignition Risk

Hyeongon Park, Daniel K. Molzahn, and Jongheon Lee

***Abstract*—In this paper, we study an integrated planning and multi-period operational problem for wildfire-resilient power grid operation, in which preventive public safety power shutoff (PSPS) decisions are taken in advance to mitigate wildfire-induced disruptions. Unlike conventional PSPS models that represent wildfire risk through exogenous parameters, we explicitly model wildfire ignition events that may damage energized transmission lines and force them out of service. This formulation captures the decision-dependent nature of wildfire risk and introduces stochastic network topology changes. We formulate the problem as a two-stage stochastic optimization model that minimizes the expected operational and wildfire damage costs under ignition-driven disruption scenarios. Because scenario probabilities depend on PSPS decisions, the resulting problem is a mixed-integer nonlinear program (MINLP). To solve this model efficiently, we derive an exact linear representation of decision-dependent scenario probabilities and develop a mixed-integer linear programming (MILP)-based bounding framework. Computational experiments on representative transmission systems demonstrate that the proposed approach yields different PSPS strategies from conventional risk-based formulations, while achieving high solution accuracy with significantly improved computational scalability relative to the original MINLP. The results further indicate that network recourse can provide additional operational benefits under wildfire disruptions.**

***Index Terms*—Public safety power shutoff (PSPS), decision-dependent uncertainty, wildfire ignition risk, network topology control, stochastic optimization**

NOMENCLATURE

Sets and Indices:

$\mathcal{B}$	Set of buses, indexed by i.
$\mathcal{G}$	Set of generators, indexed by g.
$\mathcal{D}$	Set of load demands, indexed by d.
$\mathcal{L}$	Set of transmission lines, indexed by ℓ.
$\mathcal{T}$	Set of time periods ($\mathcal{T} = \{1, \ldots, T\}$), indexed by t.
$\mathcal{S}$	Set of wildfire scenarios, indexed by s.
$\mathcal{B}^{\text{cand}}$	Subset of buses equipped with switching capability for busbar splitting.
$\mathcal{G}_i$	Set of generators at bus i.
$\mathcal{D}_i$	Set of load demands at bus i.
$\mathcal{E}_i$	Set of incident line-end pairs (ℓ, e) connected to bus i.
e	Line-end index ($e \in \{\text{fr}, \text{to}\}$).

Parameters:

X_ℓ	Reactance of line ℓ.
$F_\ell^{\max}$	Thermal flow limit of line ℓ.
p_ℓ	Baseline wildfire ignition probability of line ℓ.
w_ℓ^s	Wildfire state of line ℓ in scenario s (1 intact, 0 damaged).
$P_{d,t}$	Active power demand of load d at time t.
$P_g^{\min}$	Minimum active power output of generator g.
$P_g^{\max}$	Maximum active power output of generator g.
c_g	Marginal generation cost of generator g.
c_d^{voll}	Value of lost load (VOLL) of demand d.
c_ℓ^{fire}	Wildfire damage cost coefficient of line ℓ.
$\theta^{\max}$	Big-M constant for busbar phase-angle coupling.
M_ℓ	Big-M constant for DC power flow constraints.
M_θ	Big-M constant for line-end angle linkage.
$N_{\text{split}}^{\max}$	Maximum number of buses allowed to be split in each scenario.
$i_{\ell,e}$	Bus index associated with line-end (ℓ, e).
$\sigma_{\ell,e,i}$	Incidence parameter: $+1$ if line-end (ℓ, e) injects power into bus i, -1 if it withdraws, and 0 otherwise.

Binary Decision Variables:

z_ℓ	PSPS decision for line ℓ (1 energized, 0 de-energized).
y_ℓ^s	Line availability in scenario s after wildfire realization (1 available, 0 unavailable).
h_i^s	Busbar configuration at bus i in scenario s (1 merged, 0 split).
h_g^s	Busbar assignment of generator g in scenario s.
h_d^s	Busbar assignment of demand d in scenario s.
$h_{\ell,e}^s$	Busbar selection for line ℓ at end e in scenario s.

Continuous Decision Variables:

$p_{g,k,t}^s$	Active power output of generator g assigned to busbar $k \in \{1, 2\}$ at time t in scenario s.
$p_{d,k,t}^s$	Served load of demand d on busbar $k \in \{1, 2\}$ at time t in scenario s.
$l_{d,t}^s$	Load shedding amount of demand d at time t in scenario s.
$f_{\ell,t}^s$	Total power flow on line ℓ at time t in scenario s.
$f_{\ell,e,k,t}^s$	Power flow of line ℓ at end e connected to busbar k at time t in scenario s.
$\theta_{i,k,t}^s$	Phase angles at bus i on busbar $k \in \{1, 2\}$ at time t in scenario s.
$\theta_{\ell,e,t}^s$	Phase angle at line-end e of line ℓ at time t in scenario s.

School of Systems Management and Safety Engineering, Pukyong National University, Busan, 48516, South Korea (e-mail: hyeongon@pknu.ac.kr)

School of Electrical and Computer Engineering, Georgia Institute of Technology, Atlanta, GA, 30313, USA (e-mail: molzahn@gatech.edu)

Department of Industrial and Management Engineering, Incheon National University, Incheon, 22012, South Korea (e-mail: jongheon@inu.ac.kr)

I. Introduction

In recent years, wildfires have posed an escalating threat to electric power systems, particularly in regions such as California and Australia that are increasingly exposed to extreme heat, prolonged drought, and strong winds. Electrical infrastructure, such as overhead transmission and distribution lines, is a major source of wildfire ignitions, especially under red flag weather conditions [1]. To mitigate this risk, many utilities have adopted Public Safety Power Shutoff (PSPS) programs, which proactively de-energize selected grid components during periods of elevated wildfire risk to prevent equipment-related ignitions [2]. While PSPS actions can significantly reduce wildfire hazards, they may also lead to substantial operational and societal disruptions, including widespread service interruptions, load curtailments, disruptions to critical infrastructure, and large-scale economic losses [3].

The inherent trade-off between wildfire mitigation and power system reliability has motivated a growing body of research on optimization-based decision support for PSPS planning and operation. Early work proposed mathematical optimization frameworks for determining preventive line de-energization strategies that balance wildfire risk reduction and load delivery under power flow constraints [4]. Subsequent studies extended these formulations by incorporating additional operational considerations such as restoration planning [5], generator commitment decisions [6], and network topology control [7]. Other research has investigated complementary aspects of PSPS decision-making, including the scheduling of PSPS events based on stochastic weather observations [8] and fairness considerations in the allocation of outage impacts across communities [9].

More recently, stochastic and risk-aware optimization frameworks have been proposed to capture uncertainty in wildfire conditions and their operational impacts. For example, risk-averse formulations balance wildfire damages and PSPS-induced outages under uncertain environmental conditions [10], while stochastic models represent wildfire-induced disruptions to power system components and guide preventive grid operation [11], [12]. Beyond such stochastic representations, recent work has explored optimization-based modeling of wildfire spread dynamics to identify high-impact outage scenarios under adverse conditions [13]. Despite these advances, most existing approaches represent wildfire risk through exogenous parameters or scenario-based damage models, where ignition probabilities and disruption events are specified independently of the operator's preventive actions.

In this context, decision-dependent uncertainty (DDU), in which uncertainty depends on operational or planning decisions, has recently attracted increasing attention in power system optimization as a means to address the limitations of exogenous or scenario-based representations [14]. In wildfire-resilient power systems, several studies have begun to incorporate decision-dependent wildfire risks. For example, Pianco et al. [15] developed a stochastic planning framework in which transmission line failure probabilities depend on operational conditions such as power flows and infrastructure investments. Similarly, Greenough et al. [16] proposed a distributionally robust PSPS model in which outage probabilities depend on de-energization decisions. However, these approaches capture decision dependence primarily through adjustments of outage probabilities or risk parameters, while the operational availability of transmission lines remains determined solely by preventive decisions.

In practice, wildfire ignition is a physical process that may damage energized transmission lines and force them out of service. Motivated by this observation, this paper develops a stochastic optimization framework that explicitly captures the interaction between PSPS decisions and wildfire-induced transmission line outages. In the proposed formulation, energizing a transmission line exposes it to wildfire ignition risk, whereas de-energizing the line eliminates this risk. If ignition occurs on an energized line, the line may become damaged and subsequently be removed from service. Consequently, the model distinguishes among three possible states for each transmission line: intentionally de-energized, energized and intact, or energized but damaged due to wildfire ignition. This modeling perspective captures the decision-dependent nature of wildfire risk and introduces stochastic network topology in which line availability depends on both preventive actions and ignition-induced outages.

To account for the consequences of such disruptions, the model integrates preventive PSPS decisions with multi-period operational recourse under the resulting network topology. Because wildfire-induced outages and preventive line de-energizations may significantly reduce the number of available transmission lines, topology control actions such as bus-bar splitting [17], [18] are incorporated to better utilize the remaining network resources and maintain feasible grid operations.

The resulting optimization problem takes the form of a two-stage stochastic program with decision-dependent scenario probabilities. Since scenario probabilities depend on first-stage PSPS decisions, the formulation leads to a nonconvex mixed-integer nonlinear program (MINLP) involving bilinear coupling between decision variables and scenario probabilities. To address this computational challenge, we develop an exact reformulation and a mixed-integer linear programming (MILP)-based bounding framework that enables efficient solution using commercial MILP solvers.

The main contributions of this paper are summarized as follows:

- We develop a stochastic PSPS optimization model that explicitly captures wildfire ignition-driven transmission line outages. Unlike conventional formulations in which PSPS decisions directly determine line availability or modify failure probabilities, the proposed model represents wildfire ignition as a stochastic physical process that can damage energized transmission lines, thereby introducing decision-dependent network availability.
- We integrate preventive PSPS decisions with operational recourse under stochastic network topology and incorporate topology control actions, including bus-bar splitting, to better utilize limited transmission resources under wildfire-induced disruptions.
- We derive an exact linear representation of decision-dependent scenario probabilities and propose a MILP-

based bounding framework to efficiently solve the resulting nonconvex MINLP.
- We evaluate the proposed framework on representative transmission systems under various wildfire scenarios. Numerical experiments show that the proposed model yields different PSPS strategies compared with conventional risk-based formulations, while achieving high solution accuracy with significantly improved computational scalability. The results further demonstrate the operational benefits of incorporating network recourse actions.

The rest of the paper is organized as follows. Section II presents the problem definition and formulates the integrated planning and operational model under decision-dependent wildfire risk. Section III introduces the proposed solution framework, including the exact linearization of scenario probabilities and the MILP-based bounding approach. Section IV reports numerical experiments and discusses the performance of the proposed methods. Finally, Section V concludes the paper and outlines directions for future research.

II. Problem Definition and Mathematical Formulation

A. Problem Definition

In this paper, we consider an integrated planning and multi-period operation problem under wildfire risk, in which preventive PSPS actions are used to mitigate the likelihood and impact of wildfire-induced outages. Prior to an operational day during which wildfire ignition events may occur, the system operator determines which transmission lines remain energized and which are intentionally de-energized. These PSPS decisions remain fixed over the subsequent operational horizon. After the PSPS decisions are implemented, wildfire conditions are realized as stochastic ignition outcomes that may damage energized transmission lines.

Wildfire uncertainty is represented by a finite set of scenarios $\mathcal{S}$, each describing a possible realization of wildfire ignition outcomes across transmission lines. For each line $\ell \in \mathcal{L}$ and scenario $s \in \mathcal{S}$, the parameter $w_\ell^s = 1$ indicates that line ℓ remains intact after the wildfire realization, whereas $w_\ell^s = 0$ indicates that the line is damaged and therefore unavailable for power transfer. Let $p_\ell \in [0,1]$ denote the baseline wildfire ignition probability associated with line ℓ, reflecting exogenous wildfire risk conditions. Throughout this work, wildfire ignition events are assumed to be independent across transmission lines [16], [19].

A key feature of the problem is that PSPS decisions influence wildfire ignition risk and therefore affect the likelihood of different post-wildfire network configurations. In particular, energizing a transmission line exposes it to wildfire ignition risk with probability p_ℓ, whereas de-energizing the line eliminates this ignition risk. Consequently, the availability of each transmission line after wildfire realization depends both on preventive PSPS actions and on stochastic ignition events.

After wildfire conditions are realized, the operator determines recourse actions to operate the system over the planning horizon under the resulting network topology. The planning horizon can be interpreted as the period during which PSPS actions remain in effect until service restoration becomes possible (e.g., after inspection and safety clearance), during which operational costs accumulate under reduced network availability. A transmission line can be used for power transfer only if it is energized in the first stage and remains intact in the realized scenario. These recourse decisions include generator dispatch, power flows, phase angles under a DC approximation, and load shedding. In addition, the operator can further adjust the network topology through recourse actions such as substation reconfiguration and line switching to better utilize available resources under wildfire-induced network limitations [18]. The overall objective is to determine PSPS and operational recourse actions that minimize the expected operating cost under wildfire uncertainty.

B. Decision-Dependent Scenario Probabilities

We now formally model how PSPS decisions induce decision-dependent wildfire scenario probabilities. Under the independence assumption introduced in Section II-A, the probability of each wildfire scenario $s \in \mathcal{S}$ can be expressed as the product of line-wise survival or outage probabilities. Specifically, the probability of scenario s is given by

$$\pi_s = \prod_{\ell \in \mathcal{L}} q_{s,\ell},$$

where $q_{s,\ell}$ denotes the probability contribution of line $\ell \in \mathcal{L}$ under scenario $s \in \mathcal{S}$.

The contribution $q_{s,\ell}$ depends on both the PSPS decision and the wildfire realization. Let $z_\ell \in \{0,1\}$ denote the PSPS decision for line ℓ, where $z_\ell = 1$ indicates that the line remains energized and $z_\ell = 0$ indicates that it is intentionally de-energized. Recall that the scenario parameter $w_\ell^s \in \{0,1\}$ indicates whether the line remains intact in scenario s. The value 1 therefore consistently represents an available line state for both z_ℓ and w_ℓ^s.

Given the baseline ignition probability p_ℓ, the probability contribution of line ℓ under scenario s can be written as

$$\begin{aligned} q_{s,\ell} &= \begin{cases} p_\ell, & \text{if } z_\ell = 1 \text{ and } w_\ell^s = 0, \\ 1 - p_\ell, & \text{if } z_\ell = 1 \text{ and } w_\ell^s = 1, \\ w_\ell^s, & \text{if } z_\ell = 0, \end{cases} \\ &= (p_\ell - 2p_\ell w_\ell^s)\, z_\ell + w_\ell^s, \qquad \forall s \in \mathcal{S},\ \forall \ell \in \mathcal{L}. \end{aligned} \tag{1}$$

The affine expression in (1) provides a compact representation of the above piecewise relationship and is valid because z_ℓ is binary. Substituting this expression into the product form yields the decision-dependent probability of scenario s:

$$\pi_s(\mathbf{z}) \;=\; \prod_{\ell \in \mathcal{L}} \Big((p_\ell - 2p_\ell w_\ell^s) z_\ell + w_\ell^s \Big), \qquad s \in \mathcal{S}. \tag{2}$$

C. Operational Constraints Considering Network Topology Control

Using the decision-dependent scenario probabilities $\pi_s(\mathbf{z})$ derived in the previous subsection, we now formulate the operational model under PSPS actions and wildfire scenarios. The PSPS decisions z_ℓ constitute first-stage binary variables that remain fixed throughout the planning horizon, while all

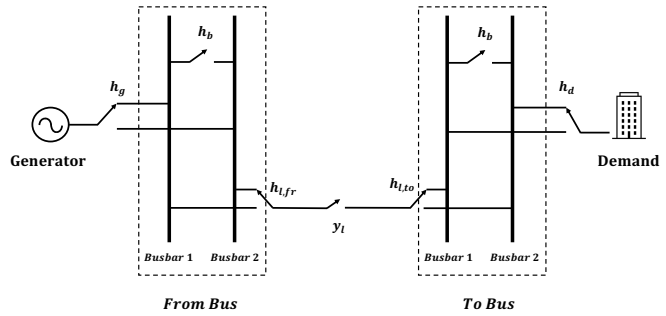

Fig. 1. Illustration of bus splitting and switching [20]

other operational decisions are determined in the recourse stage for each scenario $s \in \mathcal{S}$ and time period $t \in \mathcal{T}$.

The following constraints describe the resulting system operation under stochastic network availability.

First, constraints (3a) and (3b) define the scenario-dependent availability of each line by combining PSPS decisions and wildfire-induced outages:

$$y_\ell^s \le z_\ell, \tag{3a}$$
$$y_\ell^s \le w_\ell^s. \tag{3b}$$

When $z_\ell = 1$ and $w_\ell^s = 1$, y_ℓ^s is a scenario-dependent recourse decision that allows additional line de-energization for topology control.

To increase operational flexibility under reduced network availability, we allow topology control through substation reconfiguration. Specifically, each physical bus $i \in \mathcal{B}$ is split into two busbars indexed by $k \in \{1, 2\}$. The resulting bus splitting and switching mechanism is illustrated in Fig. 1.

Next, we assume that only a subset of buses $\mathcal{B}^{\text{cand}}$ possesses switching capabilities as in (3c); for all other buses, the two busbars remain permanently merged. Binary variables h_i^s, h_g^s, and h_d^s determine bus splitting and the assignment of generators and loads to busbars in each scenario.

$$h_i^s = 1 \quad \forall i \in \mathcal{B} \setminus \mathcal{B}^{\text{cand}}. \tag{3c}$$

Constraint (3d) enforces the merge/split decision at each bus, where the two busbars share the same phase angle when merged.

$$-\theta^{\max}(1 - h_i^s) \le \theta_{i,1,t}^s - \theta_{i,2,t}^s \le \theta^{\max}(1 - h_i^s). \tag{3d}$$

Constraints (3e) and (3f) model the assignment of each generator to one of the two busbars.

$$P_g^{\min}(1 - h_g^s) \le p_{g,1,t}^s \le P_g^{\max}(1 - h_g^s), \tag{3e}$$
$$P_g^{\min} h_g^s \le p_{g,2,t}^s \le P_g^{\max} h_g^s, \tag{3f}$$

Constraints (3g)–(3j) describe load assignment to busbars and allowable load shedding.

$$0 \le p_{d,1,t}^s \le P_{d,t}(1 - h_d^s), \tag{3g}$$
$$0 \le p_{d,2,t}^s \le P_{d,t} h_d^s, \tag{3h}$$
$$0 \le l_{d,t}^s \le P_{d,t}, \tag{3i}$$
$$p_{d,1,t}^s + p_{d,2,t}^s + l_{d,t}^s = P_{d,t}. \tag{3j}$$

The following constraints (3k)–(3o) enforce thermal limits and busbar selection for transmission lines.

$$-F_\ell^{\max} y_\ell^s \le f_{\ell,t}^s \le F_\ell^{\max} y_\ell^s, \tag{3k}$$
$$f_{\ell,t}^s = f_{\ell,\text{fr},1,t}^s + f_{\ell,\text{fr},2,t}^s = f_{\ell,\text{to},1,t}^s + f_{\ell,\text{to},2,t}^s, \tag{3l}$$
$$-F_\ell^{\max}(1 - h_{\ell,e}^s) \le f_{\ell,e,1,t}^s \le F_\ell^{\max}(1 - h_{\ell,e}^s), \tag{3m}$$
$$-F_\ell^{\max} h_{\ell,e}^s \le f_{\ell,e,2,t}^s \le F_\ell^{\max} h_{\ell,e}^s, \tag{3n}$$
$$h_{\ell,e}^s \le y_\ell^s. \tag{3o}$$

Constraints (3p) and (3q) link each line-end angle to the selected busbar angle.

$$-M_\theta h_{\ell,e}^s \le \theta_{\ell,e,t}^s - \theta_{i_{\ell,e},1,t}^s \le M_\theta h_{\ell,e}^s, \tag{3p}$$
$$-M_\theta(1 - h_{\ell,e}^s) \le \theta_{\ell,e,t}^s - \theta_{i_{\ell,e},2,t}^s \le M_\theta(1 - h_{\ell,e}^s). \tag{3q}$$

Constraint (3r) enforces the DC power flow relationship when the transmission line is available.

$$-M_\ell(1 - y_\ell^s) \le f_{\ell,t}^s - \frac{1}{X_\ell}\left(\theta_{\ell,\text{fr},t}^s - \theta_{\ell,\text{to},t}^s\right) \le M_\ell(1 - y_\ell^s). \tag{3r}$$

Finally, constraints (3s) and (3t) enforce power balance at each busbar, while constraint (3u) limits the number of split buses available for topology control.

$$\sum_{g \in \mathcal{G}_i} p_{g,1,t}^s - \sum_{d \in \mathcal{D}_i} p_{d,1,t}^s = \sum_{(\ell,e) \in \mathcal{E}_i} \sigma_{\ell,e,i} f_{\ell,e,1,t}^s, \tag{3s}$$
$$\sum_{g \in \mathcal{G}_i} p_{g,2,t}^s - \sum_{d \in \mathcal{D}_i} p_{d,2,t}^s = \sum_{(\ell,e) \in \mathcal{E}_i} \sigma_{\ell,e,i} f_{\ell,e,2,t}^s, \tag{3t}$$
$$\sum_{i \in \mathcal{B}^{\text{cand}}} (1 - h_i^s) \le N_{\text{split}}^{\max}, \tag{3u}$$
$$z_\ell,\, y_\ell^s,\, h_i^s,\, h_g^s, h_d^s,\, h_{\ell,e}^s \in \{0, 1\}. \tag{3v}$$

D. Objective Function and Model Formulation

The scenario-wise costs consist of operational and wildfire damage costs. First, the operational cost for scenario s and time period t consists of variable generation costs and load shedding penalties, and is given by

$$C_{s,t}^{\text{op}}(\mathbf{x}) := \sum_{g \in \mathcal{G}} c_g p_{g,t}^s + \sum_{d \in \mathcal{D}} c_d^{\text{voll}} l_{d,t}^s. \tag{4}$$

Here, $\mathbf{x}$ denotes the continuous decision variables associated with system operation.

The wildfire damage cost incurred in scenario s under PSPS decisions $\mathbf{z}$ is defined as

$$C_s^{\text{fire}}(\mathbf{z}) = \sum_{\ell \in \mathcal{L}} c_\ell^{\text{fire}}\, z_\ell\, (1 - w_\ell^s)\,. \tag{5}$$

This term accounts for wildfire damage caused by energized transmission lines, i.e., lines for which no preventive PSPS action has been applied.

Using the cost definitions in (4) and (5), the overall optimization problem can be written compactly as

$$(P) \quad \min_{\mathbf{z},\,\mathbf{p},\,\boldsymbol{\theta},\,\mathbf{l},\,\mathbf{f}} \quad \sum_{s \in \mathcal{S}} \pi_s(\mathbf{z}) \left(\sum_{t \in \mathcal{T}} C_{s,t}^{\text{op}}(\mathbf{x}) + C_s^{\text{fire}}(\mathbf{z}) \right)$$
$$\text{s.t.} \quad \text{Constraints (3a)–(3v).}$$

Problem (P) is a mixed-integer nonlinear program (MINLP) because the expected-cost objective multiplies scenario-dependent operational and wildfire damage costs by the decision-dependent scenario probabilities $\pi_s(\mathbf{z})$. This structure

results in multilinear terms such as $\pi_s(\mathbf{z})\, p^s_{g,t}$, $\pi_s(\mathbf{z})\, l^s_{d,t}$, and $\pi_s(\mathbf{z})\, z_\ell$, which make the problem difficult to solve directly using off-the-shelf optimization solvers. This motivates the development of the solution approach presented in the next section.

III. Solution Approach

In this section, we develop an efficient solution framework for Problem (P) that can be handled by commercial solvers. First, we derive an exact linear representation of the decision-dependent scenario probabilities in Section III-A. Second, we reformulate the remaining probability–cost bilinearities via probability discretization, which leads to a MILP-based bounding scheme in Section III-B. Finally, we describe implementation details in Section III-C.

A. Linearization of Scenario Probabilities

The decision-dependent probability $\pi_s(\mathbf{z})$ is a multilinear product of binary-dependent terms, which is difficult to handle directly in off-the-shelf solvers. To obtain an exact yet tractable representation, we propose a line-wise linearization that represents $\pi_s(\mathbf{z})$ as a continuous variable subject to linear constraints.

Recall that the scenario probability can be written as $\pi_s(\mathbf{z}) = \prod_{\ell\in\mathcal{L}} q_{s,\ell}$, where each term $q_{s,\ell}$ depends on the PSPS decision z_ℓ and the scenario realization w^s_ℓ. To linearize this product, we introduce auxiliary variables that recursively accumulate these contributions.

Let $r_{s,\ell}$ denote the cumulative probability up to line ℓ in scenario s, i.e., the partial product of the first ℓ terms, so that $\pi_s(\mathbf{z}) = r_{s,|\mathcal{L}|}$. We initialize the recursion as

$$r_{s,0} = 1, \qquad \forall s \in \mathcal{S}, \tag{6a}$$
$$0 \le r_{s,\ell} \le 1, \qquad \forall s \in \mathcal{S},\ \forall \ell \in \mathcal{L}, \tag{6b}$$

and update it sequentially across lines.

For each line ℓ, the contribution $q_{s,\ell}$ takes different values depending on z_ℓ and w^s_ℓ: when $z_\ell = 1$, it equals either p_ℓ or $1 - p_\ell$, and when $z_\ell = 0$, it reduces to w^s_ℓ. This piecewise relationship can be written in affine form as in (1). Using this representation, the cumulative probability can be expressed recursively as

$$r_{s,\ell} = w^s_\ell\, r_{s,\ell-1} + p_\ell(1-2w^s_\ell)\, t_{s,\ell}, \qquad \forall s \in \mathcal{S},\ \forall \ell \in \mathcal{L}, \tag{7}$$

where $t_{s,\ell} = z_\ell r_{s,\ell-1}$.

When $z_\ell = 0$, the recursion reduces to $r_{s,\ell} = w^s_\ell r_{s,\ell-1}$, while for $z_\ell = 1$, the term $t_{s,\ell}$ activates the ignition-dependent factor, yielding the correct contribution $q_{s,\ell} r_{s,\ell-1}$. Thus, the recursion exactly reproduces the original product $\prod_\ell q_{s,\ell}$, i.e., $r_{s,\ell} = \prod_{k=1}^{\ell} q_{s,k}$.

Since z_ℓ is binary and $0 \le r_{s,\ell-1} \le 1$, the bilinear term $t_{s,\ell} = z_\ell r_{s,\ell-1}$ can be modeled exactly using the McCormick envelope [21]:

$$t_{s,\ell} \le z_\ell, \tag{8a}$$
$$t_{s,\ell} \le r_{s,\ell-1}, \tag{8b}$$
$$t_{s,\ell} \ge r_{s,\ell-1} - (1 - z_\ell), \tag{8c}$$
$$t_{s,\ell} \ge 0. \tag{8d}$$

With this construction, the decision-dependent scenario probability is given by

$$\pi_s(\mathbf{z}) = r_{s,|\mathcal{L}|}, \qquad \forall s \in \mathcal{S}. \tag{9}$$

In summary, constraints (6) and (8) provide an exact linear representation of $\pi_s(\mathbf{z})$, with no approximation in the probability itself. The remaining nonconvexity arises from its coupling with scenario-dependent costs in the objective, which motivates the MILP-based bounding approach developed next.

B. MILP Reformulation via Probability Discretization

The objective of Problem (P) contains probability–cost products of the form $\pi_s(\mathbf{z})\, C^{\text{op}}_s(\mathbf{x})$ and $\pi_s(\mathbf{z})\, C^{\text{fire}}_s(\mathbf{z})$. Although $\pi_s(\mathbf{z})$ itself can be represented exactly through (6) and (8), these probability–cost products remain nonconvex. To address this challenge, we develop a MILP-based bounding framework based on interval discretization of the probability domain and interval-wise relaxation of the resulting bilinear objective terms.

1) Interval Partition and Selection: For each scenario $s \in \mathcal{S}$, consider a partition of the probability domain $[0, 1]$ into a finite collection of disjoint intervals,

$$\mathcal{I}_s \;:=\; \left\{ [\underline{\pi}_{s,b}, \overline{\pi}_{s,b}] \;\middle|\; b = 1, \dots, B_s \right\}, \tag{10}$$

satisfying

$$0 = \underline{\pi}_{s,1} < \overline{\pi}_{s,1} = \underline{\pi}_{s,2} < \cdots < \overline{\pi}_{s,B_s} = 1. \tag{11}$$

We associate each interval b with a binary selection variable $\delta_{s,b} \in \{0, 1\}$ and require that exactly one interval be selected:

$$\sum_{b=1}^{B_s} \delta_{s,b} = 1, \qquad \forall s \in \mathcal{S}. \tag{12}$$

Then, when interval b is selected, the decision-dependent probability $\pi_s(\mathbf{z})$ lies in the selected interval as

$$\sum_{b=1}^{B_s} \underline{\pi}_{s,b}\, \delta_{s,b} \le \pi_s(\mathbf{z}) \le \sum_{b=1}^{B_s} \overline{\pi}_{s,b}\, \delta_{s,b}, \quad \forall s \in \mathcal{S}. \tag{13}$$

Note that these constraints do not modify the exact recursive definition of $\pi_s(\mathbf{z})$ given by (6)–(9); instead, they restrict each probability to a selected interval, enabling tighter relaxations of probability–cost products.

2) Obtaining Lower and Upper Bounds: Under interval containment, define the selected lower endpoint as

$$\underline{\pi}_s(\boldsymbol{\delta}) \;:=\; \sum_{b=1}^{B_s} \underline{\pi}_{s,b}\, \delta_{s,b}. \tag{14}$$

Then, for each scenario $s \in \mathcal{S}$, we obtain the lower bound

$$\pi_s(\mathbf{z}) \Big(\sum_{t\in\mathcal{T}} C^{\text{op}}_{s,t}(\mathbf{x}) + C^{\text{fire}}_s(\mathbf{z}) \Big) \ge \underline{\pi}_s(\boldsymbol{\delta}) \Big(\sum_{t\in\mathcal{T}} C^{\text{op}}_{s,t}(\mathbf{x}) + C^{\text{fire}}_s(\mathbf{z}) \Big). \tag{15}$$

Thus, we can construct an optimization model (16) whose optimal objective value is a lower bound of (P).

$$\begin{aligned} \min_{\mathbf{z},\,\mathbf{p},\,\boldsymbol{\theta},\,\mathbf{l},\,\mathbf{f}} \quad & \sum_{s\in\mathcal{S}} \underline{\pi}_s(\boldsymbol{\delta}) \Big(\sum_{t\in\mathcal{T}} C^{\text{op}}_{s,t}(\mathbf{x}) + C^{\text{fire}}_s(\mathbf{z}) \Big) \\ \text{s.t.} \quad & \text{Constraints (3a)–(3v)} \\ & \text{Constraints (12)–(13).} \end{aligned} \tag{16}$$

Here, the objective function in (16) involves products between binary variables $\delta_{s,b}$ and continuous cost terms. These products can be linearized using standard McCormick-type inequalities, yielding a mixed-integer linear program referred to as the *lower-bounding MILP*.

We next describe how to obtain a primal solution, and thus an upper bound, from the lower-bounding MILP. Let $(\mathbf{z}^{\mathrm{LB}}, \mathbf{x}^{\mathrm{LB}})$ be an optimal solution of the lower-bounding MILP. Fixing the first-stage PSPS decisions to $\mathbf{z}^{\mathrm{LB}}$ uniquely determines the exact decision-dependent probabilities via (2):

$$\pi_s^{\mathrm{true}} \;:=\; \pi_s(\mathbf{z}^{\mathrm{LB}}), \quad \forall s \in \mathcal{S}. \tag{17}$$

In addition, substituting $\mathbf{z}^{\mathrm{LB}}$ for $\mathbf{z}$ in Problem (P) reduces the remaining problem to an MILP in the operational variables:

$$\begin{aligned} C_s^{op}(\mathbf{z}^{\mathrm{LB}}) := \min_{\mathbf{x}} \;& \sum_{t\in\mathcal{T}} C_{s,t}^{op}(\mathbf{x}) \\ \text{s.t.} \;& \text{ Constraints (3a)–(3v) with } \mathbf{z} = \mathbf{z}^{\mathrm{LB}}. \end{aligned} \tag{18}$$

Then, using $\boldsymbol{\pi}^{\mathrm{true}}$ and $\mathbf{z}^{\mathrm{LB}}$,

$$\mathrm{UB} := \sum_{s\in\mathcal{S}} \pi_s^{\mathrm{true}} \left(C_s^{\mathrm{op}}(\mathbf{z}^{\mathrm{LB}}) + C_s^{\mathrm{fire}}(\mathbf{z}^{\mathrm{LB}}) \right) \tag{19}$$

provides a valid upper bound on Problem (P).

C. Implementation Details

In this subsection, we describe the practical implementation of the proposed framework. Although the bounding approach admits arbitrary partitions of the probability domain $[0,1]$, we adopt an *a priori* uniform discretization as a baseline implementation because it yields a compact MILP formulation.

Specifically, we partition $[0,1]$ into B uniform subintervals of width $1/B$, where

$$B = 2^K - 1, \qquad K \in \mathbb{Z}_{++}. \tag{20}$$

For each scenario $s \in \mathcal{S}$, we introduce an integer variable $y_s \in \{0, 1, \ldots, B\}$ and define the associated interval as

$$[\underline{\pi}_s, \overline{\pi}_s] \;=\; \left[\frac{y_s}{B}, \frac{y_s+1}{B} \right]. \tag{21}$$

The exact decision-dependent probability is required to satisfy

$$\frac{y_s}{B} \;\le\; \pi_s(\mathbf{z}) \;\le\; \frac{y_s+1}{B}, \qquad \forall s \in \mathcal{S}, \tag{22}$$

which enforces interval containment while preserving the exact probability recursion.

In implementation, the integer variable y_s is used via the binary expansion

$$y_s \;=\; \sum_{k=1}^{K} 2^{k-1}\, q_{s,k}, \qquad q_{s,k} \in \{0,1\}, \tag{23}$$

which provides a compact representation of interval selection. Using the lower endpoint $\underline{\pi}_s = y_s/B$ in the objective induces binary–continuous $(\mathbf{q}\cdot\mathbf{x})$ and binary–binary $(\mathbf{q}\cdot\mathbf{z})$ product terms, which can be represented exactly using McCormick envelopes in a manner analogous to (8). Note that compared with using the interval-selection variables $\delta_{s,b}$ introduced in the previous subsection, the more compact integer variables y_s with the binary expansion variables $q_{s,k}$ reduce the model size.

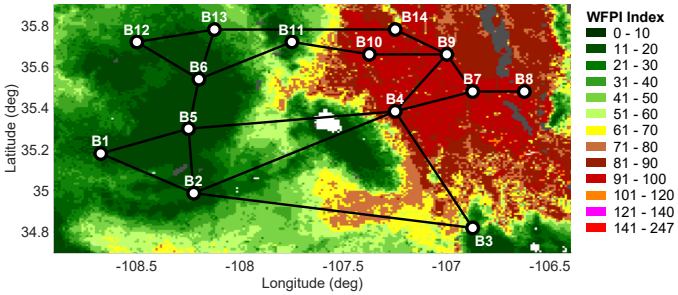

Fig. 2. Integration of the IEEE 14-bus system with geospatial wildfire risk profiles. The schematic illustrates each bus and transmission line mapped to evaluate its exposure to wildfire hazard levels. Background data represents regional WFPI values obtained from [22].

Under uniform discretization, each probability interval has width $1/B$. Consequently, the gap between the optimal objective values of the lower-bounding MILP and (P) decreases at a rate of $O(1/B)$ since

$$\left|\pi_s(\mathbf{z}) \;-\underline{\pi}_s(\boldsymbol{\delta})\right| \;\le\; \frac{1}{B}. \tag{24}$$

Thus, the lower bound obtained from the MILP becomes tighter as the discretization is refined, and the approximation error can be controlled in advance through the choice of B.

Finally, we note that the proposed framework is not restricted to uniform partitions. It can be naturally extended to iterative and progressive refinement methods, in which currently selected intervals are further subdivided based on bound gaps or incumbent solutions. Such extensions allow one to control the trade-off between approximation quality and model size.

IV. Numerical Experiment

A. Simulation Setting

1) Test System: We evaluate the proposed models on the IEEE 14-bus benchmark system from MATPOWER [23]. The system consists of 14 buses, 2 generators, and 20 transmission lines. To capture wildfire uncertainty, we consider 211 wildfire scenarios corresponding to events involving up to two simultaneous outages among the 20 lines. PSPS decisions and recourse actions are optimized over a multi-hour planning horizon with hourly time periods, and time-varying load profiles are adopted from [24]. All methods are implemented in Python and solved using Gurobi 12.0.3 [25]. All simulations were conducted on a MacBook Pro featuring an Apple M4 Pro chip with a 14-core CPU and 24 GB of unified memory. All instances were solved to a zero relative optimality gap.

2) Wildfire Probability and Damage Modeling: To characterize the spatial distribution of wildfire susceptibility, we utilize the Wildland Fire Potential Index (WFPI) from the U.S. Geological Survey [22]. As illustrated in Fig. 2, the IEEE 14-bus system is geographically mapped onto central New Mexico to extract localized WFPI telemetry data recorded on February 17, 2026. In our framework, WFPI is treated as a *relative risk indicator* rather than a probability. Accordingly, we define a line-specific wildfire risk proxy $r_\ell := \mathrm{WFPI}_\ell$.

For the proposed decision-dependent model, we normalize these proxies to construct wildfire risk weights $w_\ell = r_\ell / \sum_{k\in\mathcal{L}} r_k$, such that $\sum_{\ell\in\mathcal{L}} w_\ell = 1$ [6]. The absolute level of wildfire activity is parameterized by a parameter λ, which maps the relative risk weights to line-specific wildfire ignition probabilities via $p_\ell = 1 - e^{-\lambda w_\ell}$. This construction links the relative wildfire risk r_ℓ to line-specific ignition probabilities through a single intensity parameter λ, while enabling sensitivity analysis with respect to wildfire severity as in [26], [27]. Finally, following [28], which converts the per-acre wildfire damage estimates reported in [29] into line-level risk costs, we set the wildfire damage cost c_ℓ^{fire} to lie in the range of $\$10^5$–$\$10^6$ per line. The value of lost load (VOLL) is set to \$3000/MWh [6].

3) Risk Budget Model (Deterministic PSPS with Wildfire Risk Budget): To benchmark the proposed model, we consider a deterministic PSPS formulation commonly adopted in prior wildfire-aware power system studies (e.g., [7], [30], [31]). In this benchmark, PSPS decisions $\mathbf{z}$ are obtained by minimizing an operational objective using *decision-independent* probability for each scenario, while wildfire exposure is controlled through an explicit risk budget constraint. The benchmark adopts the same network modeling assumptions as the proposed model. The resulting MILP is formulated as

$$
\begin{aligned}
(P_{budget}) \quad \min_{\mathbf{z},\mathbf{p},\boldsymbol{\theta},\mathbf{l},\mathbf{f}} \quad & \sum_{s\in\mathcal{S}} \pi_s^0 \sum_{t\in\mathcal{T}} C_{s,t}^{\text{op}}(\mathbf{x}) \\
\text{s.t.} \quad & \text{Constraints (3a)–(3v)}, \\
& \sum_{\ell\in\mathcal{L}} r_\ell z_\ell \;\le\; R,
\end{aligned}
$$

where $C_{s,t}^{\text{op}}(\mathbf{x})$ is defined in (4) and R is the prespecified wildfire risk budget. The parameter π_s^0 denotes decision-independent scenario probability used solely to aggregate scenario-wise operational costs; in this paper, we let $\pi_s^0 = 1/|\mathcal{S}|$ for all $s \in \mathcal{S}$.

4) Test Methods: We compare three methods for obtaining PSPS decisions:

- **Benchmark**: Solve (P_{budget}), i.e., the deterministic MILP model with a wildfire risk budget.
- **MINLP**: Solve the proposed formulation in which only the scenario probabilities are linearized as in Section III-A, yielding a nonconvex MIQP (i.e., solving (P) with (6)–(9)).
- **MILP**: Replace the remaining nonlinear probability–cost terms with a mixed-integer linear reformulation and solve for the optimal PSPS decisions $\mathbf{z}$. Here, scenario probabilities are discretized using a uniform prior with $K = 14$ discretization levels.

We note that for **Benchmark** and **MILP**, the resulting PSPS decisions are fixed and re-evaluated under the full decision-dependent probability structure of Problem (P), i.e., by solving (18) with $\bar{\mathbf{z}}$.

B. Simulation Results

1) Comparison of PSPS Models Without Network Recourse Actions: To highlight the effect of the proposed decision-dependent stochastic PSPS model, we consider a simplified setting in which all network recourse actions are disallowed, i.e., neither bus splitting nor line switching is allowed, and focus on a single-period instance ($T = 1$). The wildfire intensity parameter is set to $\lambda = 0.5$, which yields a maximum line-level wildfire ignition probability of 5.93%. This relatively high-risk condition is adopted to stress-test the proposed formulations and to amplify the impact of decision-dependent wildfire probabilities, as motivated by [16]. The corresponding numerical results are summarized in Table I.

TABLE I
COMPARISON OF VARIOUS PSPS DECISION MODELS

Methods	**Benchmark** ($R = 265$)	**MINLP**	**MILP**
Total cost [\$]	148,789.2	123,941.9	123,941.9 (123,754.5)†
Operational cost [\$]	57,825.5	23,038.9	23,038.9 (22,851.5)
Wildfire cost [\$]	90,963.7	100,903.0	100,903.0 (100,903.0)
Prob. of no wildfire	0.8961	0.8555	0.8555 (0.8554)
Exp. load shed. [MW]	17.67	5.993	5.993 (5.932)
# of PSPS lines	9	7	7
Solve time [s]	[0.26, 231]††	18.36	12.14(+0.42)

† The main values in **MILP** represent the exact evaluation using the obtained PSPS decisions, while the values in parentheses report the original MILP model results.
†† For **Benchmark**, the solve time is reported as a range since the model is solved multiple times among different wildfire risk budget levels to obtain optimal budget $R = 265$.

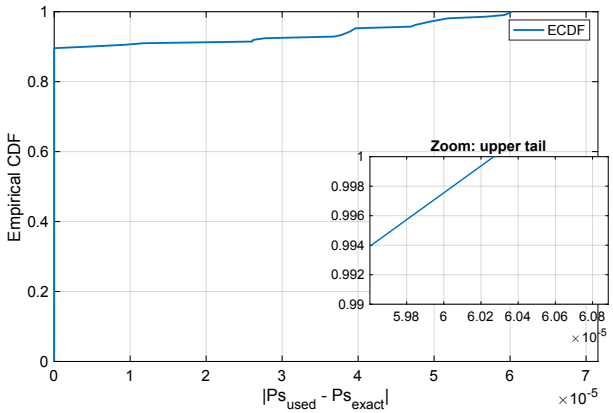

Fig. 3. Empirical CDF of the absolute error between the discretized probabilities used in the **MILP** and the exact DDU probabilities.

Under this setup, the **MILP** formulation yields identical PSPS decisions to the **MINLP** model. Although the **MILP** relies on a linearized probability approximation, its objective value is only 0.151% lower than that of the **MINLP**, demonstrating decent approximation accuracy. This is further supported by Fig. 3, which presents the empirical cumulative distribution function (CDF) of the absolute error between the discretized probabilities used in the **MILP** objective and the exact decision-dependent probabilities. As shown, the approximation errors are tightly concentrated near zero, with

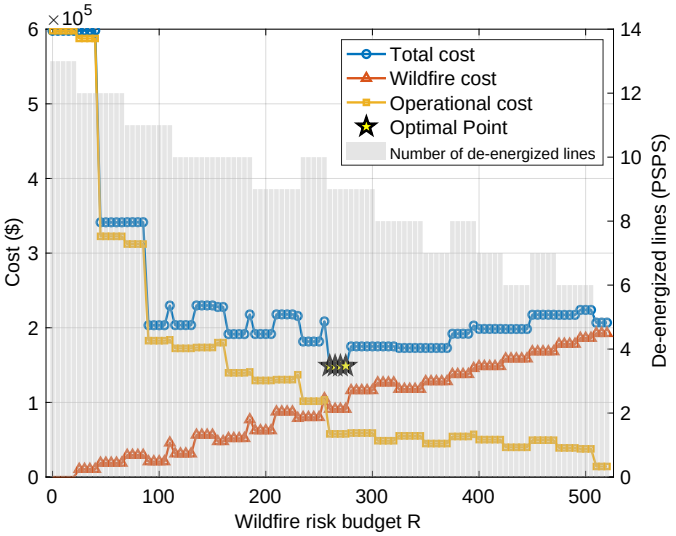

Fig. 4. PSPS decisions and expected costs of the benchmark model for various wildfire budget values.

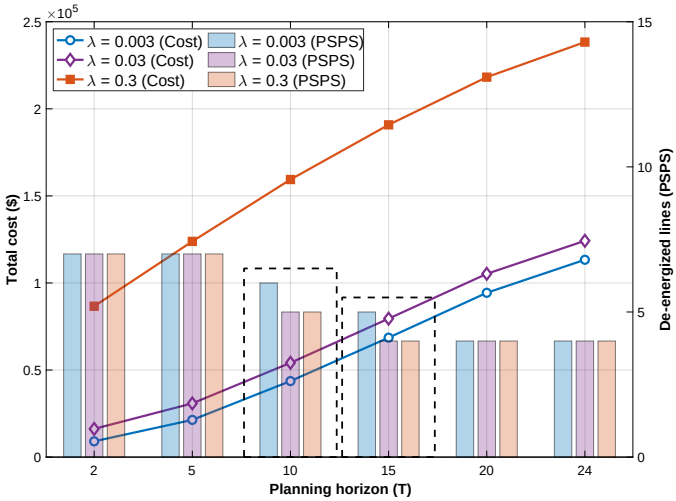

Fig. 5. Impact of wildfire occurrence intensity λ on total cost and PSPS decisions across planning horizons. The dashed box highlights a non-monotone PSPS decision at $T = 10$ and $T = 15$.

a mean of 4.1×10^{-6} and a maximum of only 6.0×10^{-5}, indicating a negligible upper-tail deviation. Moreover, when the PSPS decisions obtained from the **MILP** are fixed and re-evaluated under the full decision-dependent probability model, the resulting total cost matches that of the **MINLP** model. It should be remarked that this re-evaluation reduces to a linear program when network recourse actions are disallowed and can be completed within a fraction of a second.

We next compare the resulting PSPS decisions with a deterministic risk budget-based benchmark, which fails to recover the optimal PSPS decisions obtained by the proposed **MINLP** and **MILP** formulations. Fig. 4 illustrates the expected operational cost, wildfire cost, and total cost as functions of the wildfire risk budget R. Here, the **Benchmark** model is repeatedly solved over a wide range of R, incremented in steps of 5 to align with the discretized WFPI levels adopted in this study.

As illustrated in the bar chart in Fig. 4, the number of de-energized lines generally decreases as the wildfire risk budget R increases. Consequently, the operational cost tends to decrease due to fewer preventive shutoffs, while the wildfire cost increases as more high-risk lines remain energized. However, these trends are not strictly monotonic. Since each line possesses a distinct WFPI contribution, incremental changes in R induce non-uniform switching decisions, leading to the non-monotonic variations in both the number of de-energized lines and the associated cost components observed in the figure.

Although this trade-off yields a minimum total cost near $R = 265$, the benchmark model, even when evaluated at fine granularity, cannot identify the same optimal PSPS decisions as the proposed approaches. This discrepancy arises because the deterministic formulation relies on fixed, decision-independent risk weights that are decoupled from the actual PSPS actions. As a result, changes in line de-energization do not feed back into the modeled wildfire risk, preventing the benchmark from accurately capturing the endogenous trade-off between operational cost and wildfire exposure. This limitation ultimately results in suboptimal PSPS decisions.

Next, Fig. 5 illustrates the impact of the wildfire intensity parameter λ on the number of de-energized (PSPS) lines and the resulting total cost for various planning horizons. Here, all instances were solved using the **MILP** formulation. The intensity range considered in the experiment ($\lambda \in \{0.003, 0.03, 0.3\}$) is based on realistic daily ignition probabilities, which range approximately from 10^{-4} to 10^{-2}, as empirically modeled in [32]. In the result, as the planning horizon T increases, a general downward trend in the number of de-energized lines is observed. This occurs because PSPS actions incur cumulative operational costs, which are primarily from load shedding over longer horizons, making aggressive de-energization increasingly prohibitive. Consequently, the model favors more selective PSPS decisions.

However, a counter-intuitive result emerges at $T = 10$ and $T = 15$: as wildfire intensity λ increases from 0.003 to 0.03—and thus wildfire ignition probability p_ℓ rises—the number of PSPS actions actually decreases. This suggests that under extreme risk, additional preventive shutoffs become counterproductive. While PSPS eliminates specific ignition risks, it simultaneously increases the fragility of the residual network. If a fire-induced outage occurs on the remaining energized lines, the compounded impact of both planned (PSPS) and accidental (wildfire) outages can lead to catastrophic system failure. Consequently, the model may keep more lines energized, as the cost of additional shutoffs can outweigh the marginal benefit of further risk reduction. This highlights the importance of explicitly modeling the endogenous feedback between PSPS decisions and system-wide risk, a relationship that remains hidden when wildfire risk is treated as exogenous.

2) Impact of Network Recourse on PSPS Decisions and Operations: We evaluate the effect of network topology recourse on both PSPS decisions and post-contingency system operation in a single-period setting. Recourse actions include bus splitting and line switching. To examine how the value of recourse depends on network congestion, we consider two operating conditions in which transmission capacities are

TABLE II
COMPARISON OF PSPS DECISIONS WITH AND WITHOUT NETWORK RECOURSE ACTIONS

Metrics	80% capacity limit		75% capacity limit	
	NO RECOURSE	WITH RECOURSE	NO RECOURSE	WITH RECOURSE
Total cost [$]	175,628.7	167,093.3	189,321.7	168,314.0
Operational cost [$]	74,733.5	66,190.8	61,932.8	67,410.9
Wildfire cost [$]	100,895.3	100,902.6	127,388.8	100,903.0
Prob. of no wildfire	0.8554	0.8554	0.8323	0.8554
Exp. load shed [MW]	23.34	20.48	19.05	20.88
Solve time [s]	59.96	367.55	58.33	169.72
# of PSPS lines	7	7	6	7
PSPS decision (z^*)	11101	11101	11111	11101
	11001	11001	11001	11001
	11100	11100	11100	11100
	10110	10110	10110	10110

reduced to 80% and 75% of their nominal values. The results are summarized in Table II.

Under the 80% capacity limit, the PSPS decisions remain unchanged regardless of whether recourse actions are allowed, with 7 high-risk lines de-energized in both cases. However, enabling recourse significantly improves operational performance: the operational cost is reduced by approximately 11.4%, and expected load shedding decreases from 23.34 MW to 20.48 MW. This indicates that, even without altering preventive decisions, network recourse provides sufficient flexibility to alleviate congestion and reduce the operational burden following wildfire-induced outages.

In contrast, under more severely congested conditions (75% capacity), network recourse also affects the PSPS decisions. As shown in Table II, the model with recourse de-energizes one additional high-risk line compared to the no-recourse case, resulting in a substantial reduction in wildfire cost. This demonstrates that the availability of recourse actions can justify more aggressive preventive shutoffs, as the resulting operational flexibility mitigates their associated costs. Consequently, the optimal PSPS strategy becomes dependent on the availability of network recourse.

From a computational perspective, incorporating recourse actions increases the number of binary variables and thus the overall solution time. For example, under the 80% capacity limit, the solve time increases from 59.96 seconds to 367.55 seconds. Nevertheless, this increase reflects the expanded decision space required to capture additional operational flexibility. In practice, computational effort can be controlled by limiting the number of candidate buses for splitting or by relaxing optimality tolerances, providing a practical trade-off between solution quality and computational efficiency.

3) Computational Performance and Scalability of Solution Approaches: We evaluate the computational performance of the proposed formulations across different planning horizons and network sizes. In addition to the IEEE 14-bus system, we consider a larger IEEE 30-bus system [23] to assess scalability. The 30-bus system consists of 41 transmission lines, and a total of 541 wildfire scenarios are generated. To maintain computational tractability, multi-line wildfire scenarios are restricted to geographically proximate lines (within three buses), thereby avoiding combinatorial explosion from distant simultaneous outages. Table III reports the solution time and optimality gaps of the **MINLP** and **MILP** formulations under varying wildfire intensity levels λ and planning horizons T. A time limit of 1,800 seconds is imposed for the 14-bus system, and 7,200 seconds for the 30-bus system. When optimality is not reached within the time limit, the corresponding optimality gap is reported.

TABLE III
COMPUTATIONAL PERFORMANCE OF MINLP AND MILP METHODS

System			14-bus (20 lines, 211 scenarios)		30-bus (41 lines, 541 scenarios)	
Model	T	λ	Time [s]	Gap [%]	Time [s]	Gap [%]
MINLP	5	0.003	224.6	0	650.0	0
		0.03	1,800	<0.01	1,010.4	0
		0.3	235.4	0	6,303.6	0
	15	0.003	1,800	0.78	7,200	14.02
		0.03	1,800	0.01	7,200	<0.01
		0.3	1,800	2.94	7,200	19.18
	24	0.003	1,800	1.05	7,200	19.06
		0.03	1,800	0.16	7,200	<0.01
		0.3	1,800	4.98	7,200	21.34
MILP	5	0.003	8.1	0	45.5	0
		0.03	15.2	0	220.4	0
		0.3	121.9	0	1,016.8	0
	15	0.003	37.3	0	1,275.7	0
		0.03	92.1	0	1,087.4	0
		0.3	632.3	0	7,200	0.02
	24	0.003	77.9	0	1,627.1	0
		0.03	405.4	0	6,605.1	0
		0.3	483.4	0	7,200	0.06

Overall, the results clearly demonstrate the computational advantage of the **MILP** formulation over the **MINLP**. For the 14-bus system, the **MILP** consistently achieves global optimality across all tested values of T and λ, with solution times that remain within a few hundred seconds even for longer horizons. In contrast, while the **MINLP** formulation can solve smaller instances efficiently, its computational performance deteriorates rapidly as the planning horizon increases. In particular, for $T = 15$ and $T = 24$, most **MINLP** instances reach the time limit with non-negligible optimality gaps (up to approximately 5%), indicating difficulty in convergence.

This performance gap becomes more pronounced in larger systems. For the 30-bus case, the **MINLP** frequently fails to converge within the time limit, with optimality gaps exceeding 20%, whereas the **MILP** formulation remains stable and achieves near-optimal solutions with small gaps (typically below 0.1%).

As the planning horizon T increases, both formulations require longer solution times due to the expanded decision space and the growth in scenario-dependent variables; however, this effect is substantially more pronounced for the **MINLP**. Overall, these results demonstrate that the proposed MILP-based reformulation provides a scalable and reliable approach for

solving the decision-dependent PSPS optimization problem.

V. Conclusions

This paper presented a stochastic optimization framework for preventive PSPS planning under decision-dependent wildfire risk. The proposed model explicitly captures wildfire ignition events that may damage energized transmission lines, introducing decision-dependent stochastic network topology in which line availability depends on both preventive actions and ignition-driven disruptions. To solve the resulting two-stage stochastic program, we derived an exact linear representation of decision-dependent scenario probabilities and developed a MILP-based bounding framework for efficiently solving the resulting nonconvex MINLP. Numerical experiments show that modeling ignition-driven disruptions leads to substantially different PSPS strategies compared with conventional risk-based formulations, while the proposed MILP approximation achieves high solution accuracy and significantly improves computational efficiency. The results also demonstrate that incorporating network recourse actions, such as bus splitting, helps mitigate load shedding and operational costs when wildfire-induced outages occur.

Future research may extend the proposed framework by incorporating more detailed wildfire dynamics, such as spatial fire spread models, and by applying the methodology to larger-scale power system instances. In addition, exploring advanced decomposition or learning-based solution approaches may further improve computational performance for long-horizon planning problems.

References

[1] A. D. Syphard and J. E. Keeley, "Location, timing and extent of wildfire vary by cause of ignition," *International Journal of Wildland Fire*, vol. 24, no. 1, pp. 37–47, 2015.

[2] C. Huang, Q. Hu, L. Sang, D. D. Lucas, R. Wong, B. Wang, W. Hong, M. Yao, and V. Donde, "A review of public safety power shutoffs (PSPS) for wildfire mitigation: Policies, practices, models and data sources," *IEEE Transactions on Energy Markets, Policy and Regulation*, vol. 1, no. 3, pp. 187–197, 2023.

[3] Energy Policy Institute at the University of Chicago, "Climate-Driven Wildfires Are Reversing Clean Air Progress," Energy Policy Institute at the University of Chicago (EPIC), Tech. Rep., Aug. 2025, air Quality Life Index (AQLI) Annual Update. [Online]. Available: https://aqli.epic.uchicago.edu

[4] N. Rhodes, L. Ntaimo, and L. Roald, "Balancing wildfire risk and power outages through optimized power shut-offs," *IEEE Transactions on Power Systems*, vol. 36, no. 4, pp. 3118–3128, 2021.

[5] N. Rhodes and L. A. Roald, "Co-optimization of power line shutoff and restoration under high wildfire ignition risk," in *2023 IEEE Belgrade PowerTech*. IEEE, 2023, pp. 1–7.

[6] R. Greenough, K. Murakami, M. R. Davidson, J. Kleissl, and A. Khurram, "Wildfire resilient unit commitment under uncertain demand," *IEEE Transactions on Power Systems*, vol. 40, no. 4, pp. 3131–3143, 2025.

[7] Y. Zhou, K. Sundar, H. Zhu, and D. Deka, "Mitigating the impact of uncertain wildfire risk on power grids through topology control," in *18th International Conference on Probabilistic Methods Applied to Power Systems (PMAPS)*, 2024.

[8] A. Lesage-Landry, F. Pellerin, D. S. Callaway, and J. A. Taylor, "Optimally scheduling public safety power shutoffs," *Stochastic Systems*, vol. 13, no. 4, pp. 438–456, 2023.

[9] A. Kody, A. West, and D. K. Molzahn, "Sharing the load: Considering fairness in de-energization scheduling to mitigate wildfire ignition risk using rolling optimization," in *61st IEEE Conference on Decision and Control (CDC)*, 2022, pp. 5705–5712.

[10] J. Su, S. Mehrani, P. Dehghanian, and M. A. Lejeune, "Quasi second-order stochastic dominance model for balancing wildfire risks and power outages due to proactive public safety de-energizations," *IEEE Transactions on Power Systems*, vol. 39, no. 2, pp. 2528–2542, 2024.

[11] H. Yang, N. Rhodes, H. Yang, L. Roald, and L. Ntaimo, "Multi-period power system risk minimization under wildfire disruptions," *IEEE Transactions on Power Systems*, vol. 39, no. 5, pp. 6305–6318, 2024.

[12] R. Piansky, G. Stinchfield, A. Kody, D. K. Molzahn, and J.-P. Watson, "Long duration battery sizing, siting, and operation under wildfire risk using progressive hedging," *Electric Power Systems Research*, vol. 235, p. 110785, 2024, presented at the *23rd Power Systems Computation Conference (PSCC)*.

[13] M. Brun, X. A. Sun, and J.-P. Watson, "Modeling adversarial wildfires for power grid disruption," *arXiv:2603.18473*, March 2026.

[14] B. Wang, X. Wang, X.-P. Zhang, J. Huang, Z. Song, L. Zhang, and Y. Li, "Application of decision-dependent uncertainty in power system planning and operation analyses: A state-of-the-art review," *Electric Power Systems Research*, vol. 233, p. 110458, 2024.

[15] F. Piancó, A. Moreira, B. Fanzeres, R. Jiang, C. Zhao, and M. Heleno, "Decision-dependent uncertainty-aware distribution system planning under wildfire risk," *IEEE Transactions on Power Systems*, vol. 40, no. 6, pp. 4574–4590, 2025.

[16] R. Greenough, K. Murakami, J. Kleissl, and A. Khurram, "Optimal SVI-weighted PSPS decisions with decision-dependent outage uncertainty," *arXiv:2504.11665*, April 2025.

[17] M. Heidarifar and H. Ghasemi, "A network topology optimization model based on substation and node-breaker modeling," *IEEE Transactions on Power Systems*, vol. 31, no. 1, pp. 247–255, 2015.

[18] R. Xiao, Y. Xiang, L. Wang, and K. Xie, "Power system reliability evaluation incorporating dynamic thermal rating and network topology optimization," *IEEE Transactions on Power Systems*, vol. 33, no. 6, pp. 6000–6012, 2018.

[19] J. Yan, B. Hu, K. Xie, J. Tang, and H.-M. Tai, "Data-driven transmission defense planning against extreme weather events," *IEEE Transactions on Smart Grid*, vol. 11, no. 3, pp. 2257–2270, 2019.

[20] A. Rajaei and J. L. Cremer, "Security-constrained substation reconfiguration considering busbar and coupler contingencies," to appear in *IEEE Transactions on Power Systems*, 2026.

[21] G. P. McCormick, "Computability of global solutions to factorable nonconvex programs: Part I–Convex underestimating problems," *Mathematical Programming*, vol. 10, no. 1, pp. 147–175, 1976.

[22] U.S. Geological Survey, "Wildland Fire Potential Index," February 2025, https://www.usgs.gov/fire-danger-forecast/wildland-fire-potential-index-wfpi.

[23] R. D. Zimmerman, C. E. Murillo-Sánchez, and R. J. Thomas, "MATPOWER: Steady-state operations, planning, and analysis tools for power systems research and education," *IEEE Transactions on power systems*, vol. 26, no. 1, pp. 12–19, 2010.

[24] J. Lee, S. Lee, and K. Lee, "Multistage stochastic optimization for microgrid operation under islanding uncertainty," *IEEE Transactions on Smart Grid*, vol. 12, no. 1, pp. 56–66, 2020.

[25] Gurobi Optimization, LLC, *Gurobi Optimizer Reference Manual*, 2026. [Online]. Available: https://www.gurobi.com

[26] C. A. Graff, S. R. Coffield, Y. Chen, E. Foufoula-Georgiou, J. T. Randerson, and P. Smyth, "Forecasting daily wildfire activity using Poisson regression," *IEEE Transactions on Geoscience and Remote Sensing*, vol. 58, no. 7, pp. 4837–4851, 2020.

[27] F. Pimont, H. Fargeon, T. Opitz, J. Ruffault, R. Barbero, N. Martin-StPaul, E. Rigolot, M. Riviere, and J.-L. Dupuy, "Prediction of regional wildfire activity in the probabilistic Bayesian framework of Firelihood," *Ecological Applications*, vol. 31, no. 5, p. e02316, 2021.

[28] R. Bayani, M. Waseem, S. D. Manshadi, and H. Davani, "Quantifying the risk of wildfire ignition by power lines under extreme weather conditions," *IEEE Systems Journal*, vol. 17, no. 1, pp. 1024–1034, 2022.

[29] L. Dale, "The true cost of wildfire in the Western United States," https://www.thewflc.org/sites/default/files/TrueCostofWildfire.pdf, 2022, Western Forestry Leadership Coalition.

[30] R. Piansky, S. Taylor, N. Rhodes, D. K. Molzahn, L. A. Roald, and J.-P. Watson, "Quantifying metrics for wildfire ignition risk from geographic data in power shutoff decision-making," in *58th Hawaii International Conference on System Sciences (HICSS)*, January 2025.

[31] R. Greenough, K. Murakami, J. Kleissl, and A. Khurram, "Wildfire risk metric impact on Public Safety Power Shut-off cost savings," *arXiv:2411.10929*, November 2024.

[32] T. Keeping, S. P. Harrison, and I. C. Prentice, "Modelling the daily probability of wildfire occurrence in the contiguous United States," *Environmental Research Letters*, vol. 19, no. 2, p. 024036, 2024.